Experiments in Fluids 32 (2002) 313–325 © Springer-Verlag 2002
DOI 10.1007/s003480100359

Grain shear flow in a rotating drum

S. Longo, A. Lamberti

Abstract In the present paper we report on the experimental activities carried out on a rotating drum partially filled with grains or glass beads. The experiments give information about rheology through velocity profiles and through the velocity covariance tensor structure. We used a LDV system to measure the velocity of the grains at several points along three vertical sections. The data were also used to obtain the grain volume concentration, with encouraging results. Instantaneous velocity data were elaborated in order to obtain velocity and pseudotemperature profiles for all the experiments; for a subset of the experiments a large set of data were elaborated to obtain the velocity covariance. The velocity covariance is not collinear with the rate of deformation tensor. An attempt to justify the rotation of the tensor axes as a consequence of the kinetically induced anisotropy and of some free surface perturbations slowly moving upstream was partially successful.

1 Introduction

Granular flows are increasingly studied by many researchers. The subject in question is wide and includes flows of dry grains, of grains and fluid at different levels of concentration and of debris flows, covering applications in mechanical, chemical and civil engineering. The present understanding of the behaviour of grain particles is still not perfect, if compared with the developed studies in the field of Newtonian fluids or molecular gases. Nevertheless, the theories about the rheology of dry grain particles have been increasingly confirmed and seem to be qualitatively correct, despite the restrictive hypothesis. Experiments on granular flows are comparatively scarce; theoretical or numerical analyses are at most times restricted to idealised systems such as disks or spheres in two dimensions.

The description is either Lagrangian or Eulerian, and a particular effort is given to developing models of the granular medium as a *continuum*. Analytical and numerical approaches have provided substantial information on determining the stress tensor, the dissipation rate and the energy fluxes of the particles. Extensive reviews are by Campbell (1990), and Seminara and Tubino (1993). Jenkins and Savage (1983), followed by Lun et al. (1984), extended the dense gas theory to simulate particle behaviour in rapid granular flows, accounting for energy dissipation in nearly elastic systems. Jenkins and Richman (1986) studied either dilute or highly dense systems to the full range of the particles' elasticity coefficient. Numerical simulations of rapidly sheared granular flows (Campbell and Gong 1986; Walton and Braun 1987; Campbell 1988, 1989) were coherent with the kinetic theory.

Applications of the theory to more realistic systems were carried out by Johnson and Jackson (1987), Johnson et al. (1990), Anderson and Jackson (1992), Nott and Jackson (1992), with a close examination of proper boundary conditions (Hui et al. 1984; Jenkins and Richman 1986; Pasquarell and Ackermann 1989; Jenkins and Askari 1991; Gutt and Haff 1991).

At present, none of the available models have covered the full range of possible regimes, i.e., kinetic, collisional, frictional or quasi-static regime. Further experimental investigations are necessary to understand the physical processes, especially in the quasi-static regime.

2 Scope and objectives

The aim of the present experimental work is to provide information on stress–strain relationships, on velocity and pseudotemperature in dry rapid granular flows on an erodible bottom and in transitional flows spanning the quasi-static and collisional flow regime. Experimental studies in the collisional and quasi-static regime are quite scarce, and measuring a simple state variable such as granular temperature raises problems. Often a two-dimensional geometry is used to simplify measurements. We use a three dimensional geometry, even though our measurements are essentially limited to the particles observed through a glass that confines the motion.

Received: 23 April 1999 / Accepted: 15 July 2001

S. Longo (✉)
Department of Civil Engineering
University of Parma
Parco Area delle Scienze 181/A
43100 Parma, Italy
e-mail: sandro.longo@unipr.it
Tel.: +39-521-905157, Fax: +39-521-905924

A. Lamberti
D.I.S.T.A.R.T., University of Bologna
Viale Risorgimento 2, 40136 Bologna
Italy

This study was supported by the European Community, Debris Flow Risk Project, Contract ENV4-CT96-0253, and by MURST, Morfodinamica Fluviale e Costiera, 1997. We wish to thank Tim Chesher for polishing our English.

In order to generate a granular stream in a simple controllable manner, we used a rotating drum. Partially filled rotating drums have many practical applications in materials processing (e.g., surface polishing, grain drying); moreover, they are easy to build and to control. They are able to generate a continuous stationary grain flow characterised by all the possible regimes of motion. More often rotating drums are used in studying segregation processes. Considering the objectives of our experiments, segregation is a disturbing effect, because it modifies the flow field and the transfer mechanisms in a manner that is difficult to quantify.

We have performed measurements of the grain velocity and the grain pseudotemperature through a LDV system and obtained information about the stream profiles through video image analysis. Having detected a strong noncolinearity of the principal axes of the velocity covariance and of the rate of deformation tensor (due to nonisotropic pseudotemperature), we analyse the possible sources of anisotropy and quantify their importance. At present, the results for several experiments are available, with the drum rotating at 2 and 5 rpm half-filled with sand grains or glass beads with a diameter in the range 0.3–0.4 mm, 0.84–1.19 mm and 1.2–1.7 mm. Test conditions and material characteristics are reported in Table 1.

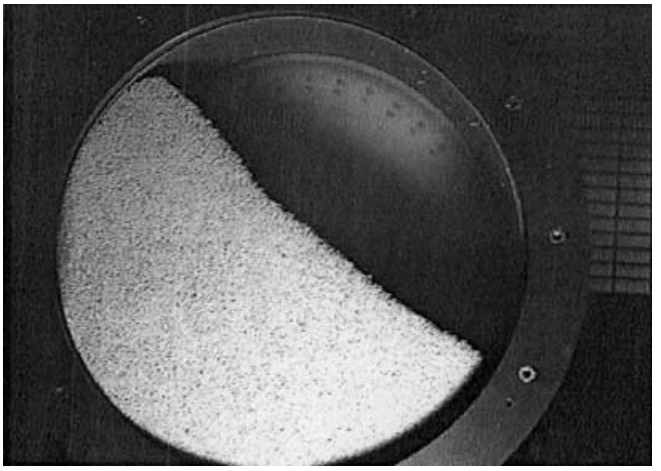

Fig. 1. Photo of the drum during rotation at 5 rpm (frame from a video)

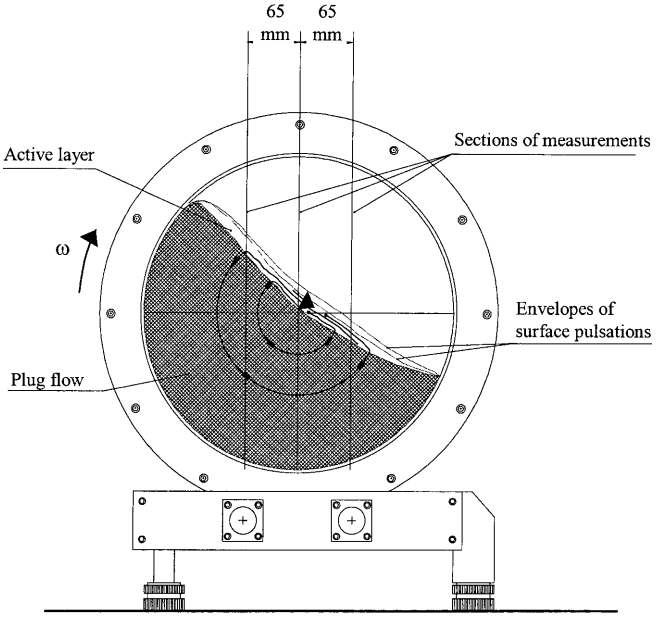

Fig. 2. Front end of the rotating drum and different regions of motion

3 Experimental set-up and measurement techniques

3.1 Experimental apparatus

The apparatus is a cylinder with a 390-mm inner diameter and 131-mm width (frontal view in Fig. 1 and Fig. 2). The cylinder is placed on a pair of friction rollers and is rotated about its axis at a constant velocity in the range 0–10 rpm by a variable-speed dc motor. The walls of the drum are made of 10-mm thick glass, which allows for optical measurements. The cylinder's inner roughness has been increased with sand paper to avoid the tendency of the whole bed to slide on the boundary as a solid body. The drum can be filled with dry grains, grains and water or any other fluid, for an analysis of grain–fluid mixture behaviour.

Three different flow regimes are observed as the rotation speed of the cylinder is increased:

– at a very low angular speed, some grains occasionally roll on the bed and avalanches occasionally develop with different amplitudes and frequency;

Table 1. Tested materials and test conditions. Sand grains B' have been obtained by sieving the material B, ϕ_r is the maximum slope angle before avalanching, ϕ_s is the slope angle after avalanching, v_o is the maximum grain volume concentration obtained under vibration

Material (mm)	ρ_s (kg/m^3)	ϕ_r (°)	ϕ_s (°)	v_o	ω (rpm)
Sand grains 1.2–1.7 (A)	2520	35.1 ± 0.2	30.9 ± 0.6	0.58	5
Sand grains 0.1	–	–	–	–	Unstable
Sand grains 0.2–0.4 (B)	–	–	–	–	Unstable
Sand grains 0.3–0.4 (B')	–	–	–	–	Unstable
Sand grains 0.84–1.19 (C)	2530	33.5 ± 0.2	30.1 ± 0.4	0.57	2–5
Glass beads 0.2–0.3	–	–	–	–	Unstable
Glass beads 0.3–0.4	2410	23.3 ± 0.2	22.5 ± 0.2	0.62	2–5

- at an intermediate angular speed, the avalanches become periodic and have an almost constant amplitude;
- at a relatively high angular speed, (greater than 1 rpm for material A, see Table 1) a stationary steady state is reached, with most of the grains moving as a solid body in a plug flow in the lower part of the drum and with a stream of variable thickness flowing down-slope above the plug.

We have investigated the latter of the three situations. Some preliminary remarks about the behaviour of the grain flow at high angular speed:

- the reached state is, on average, stationary, with a visible and recordable pulsation of the stream thickness and of the grain velocity with a time scale of a few seconds;
- a hysteresis phenomenon appears: starting from an angular speed of over 1 rpm, the periodical state is reached when the angular speed is reduced to less than 0.5 rpm;
- the glass walls always have an effect, although this is more evident at a lower angular speed;
- upstream the free surface is depressed in the stream centre, with grains moving from the glass walls towards the middle plane of the drum; the opposite happens downstream, with grains moving from the middle plane towards the glass walls.

3.2
Materials

Sand grains and glass beads of different sizes have been tested. In all the experiments, the free surface fluctuated with an amplitude equal to a few grain diameters. In some cases, the amplitude of the free-surface oscillation covered the entire flow stream, rendering the measurements meaningless; in such cases, the flow has been classified as unstable.

3.3
Measurements

We performed measurements by video-image recording and drawing on a transparent sheet placed in front of the drum to delineate the boundaries of the stream and to evaluate the time scale of the pulsation. We also used laser Doppler velocimetry (LDV) to measure the average velocity of the grains.

Measurement of the velocity of particles whose size is of the order of the measurement volume by LDV is quite unusual. Another technique is usually adopted, as suggested by Savage (1979), and successfully followed by Ahn et al. (1991) and Boateng and Barr (1997): two fibre-optic sensors are mounted in parallel at a fixed distance, and the grains passing the optical sensors generate separate signals whose cross-correlation gives the necessary information to evaluate the velocity of the grains. The reported results of such an arrangement are quite good, with a negligible error, but some disadvantages lie in the impossibility of detecting zero-velocity grains and in the intrusive nature of the probes.

In LDV systems the signal is generated by scattering a spatially modulated light (moving fringes generated by interference between two laser beams) due to moving small particles through the measurement volume, an ellipsoid with an axis of the range of 1 mm. The signal, which is collected by a photomultiplier or a photodiode, is elaborated to obtain the information. In particular, in the post-processors of the counters, the signal is filtered to detect bursts, and is then validated or rejected before further processing. The main set-up parameters are the bandwidth of the filters, which correspond to a wide or narrow range of measurable velocity, and the voltage supply of the photomultiplier, in order to optimise the signal-to-noise (S/N) ratio. The relevant outputs are the statistics of the bursts, the data rate (bursts collected per unit time) and the validation rate (ratio between the validated bursts and the collected bursts). The validation criterion is the so-called 5/8 fringe time, based on comparing the travel time of the particle through 5 and 8 fringes. The best results are obtained with very small particles (called tracers); nevertheless, we saw that even large particles scatter the laser light, first at the intersection of their leading edge with the measurement volume boundaries, then during motion through the volume with their surface roughness. It can be assumed that the effects of rotation of the particles are statistically eliminated in the average velocity, whereas they remain included in fluctuations.

We have tested the reliability of the output signal and the reliability of the measuring system by measuring the velocity of grains glued on a sheet fixed on the rotating drum. The agreement between the theoretical value and the measured value was greater than 2%. It should be noted that the rotation of the drum is not controlled by a feedback system, and small oscillations of the rotation rate with a relative amplitude of $\sim$2% and a positive drift of $\sim$1% (after 3 h) were measured. More accurate control of the rotation rate is possible, but is not substantially necessary to equalise the level of accuracy of all the measured or imposed variables.

The sample for each measurement location is of 12,000 validated bursts for both horizontal and vertical velocity components; in all cases, the interval of measurements was at least 60 s. This last restriction was imposed to average some non-stationary phenomena with a time scale of a few seconds.

4
Qualitative description of the flow

Before the presentation of the results, it is useful to describe the motion of the grains in the different regions. Our drum is half filled with grains; during motion at 5 rpm a plug flow develops in the lower part (Fig. 3 and Fig. 4), with grains packed and moving in a circular path around the axis of rotation. Their velocity is geometrically established as ωr, where r is the distance from the axis.

Over the plug flow lies the flowing layer; in the tested configuration all the particles arrive sooner or later in the flowing layer, a shearing region whose discharge increases from zero upstream to a maximum near the cylinder axis and decreases to zero downstream. With a value of the filling ratio (the ratio between the volume

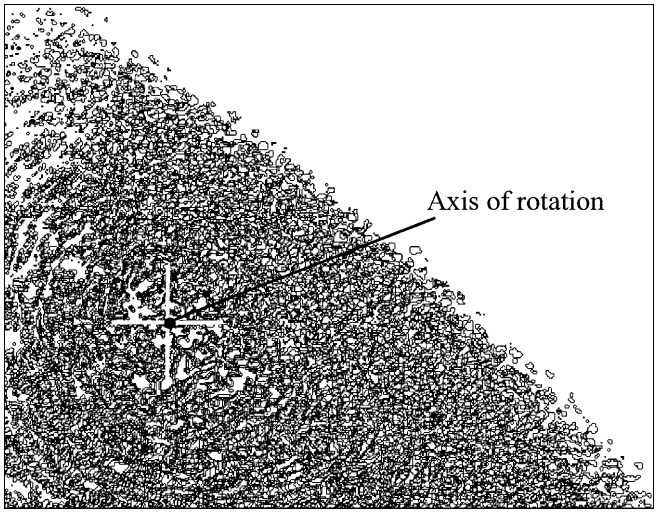

Fig. 3. Composition of four frames corresponding to the axis of rotation, 25 frames/s video

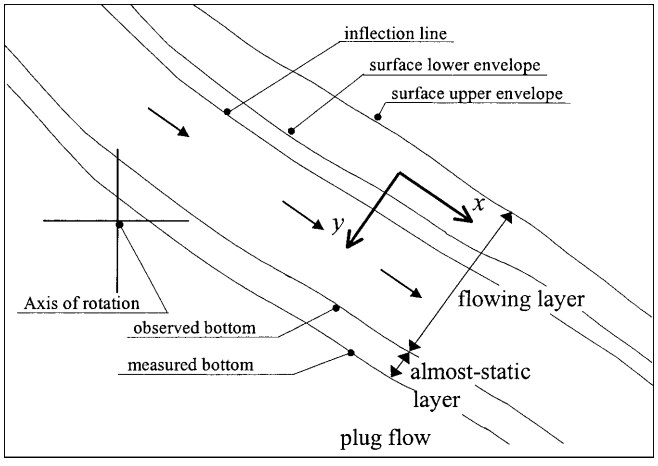

Fig. 4. Reference system and layers classification

occupied by the grains and the total internal volume of the drum) higher than ~0.5, a core of inactive grains can be noted that are simply animated by a rotation movement around the axis. The upper end of the active layer is formed by grains detached from the internal wall of the drum and ready to start rolling and shearing as soon as the local bed inclination becomes greater than the static angle of repose. Moving towards the axis, the stream normally increases its thickness; the discharge increases due to the contribution of grains whose paths intersect the interface between the plug region and the active layer. The inclination of the interface progressively reduces its value.

The maximum discharge is reached where the active layer is the nearest to the rotation axis and has a value equal to:

$$Q = \rho_s v_o \frac{\omega}{2}\left(R^2 - r^2\right) \tag{1}$$

per unit width of the drum:

ρ_s mass density of the grains;

v_o concentration of the sediments in the plug flow region;

R internal radius of the drum;

r minimum distance of the active layer bottom from the rotation axis.

Below the axis, the stream does not have enough energy to carry all the grains. The grains near the bottom reduce their velocity while the concentration increases up to the allowed limit of interparticle–interparticle movement and the particles return to the plug flow. Below the flowing layer, an undefined area exists that is occupied by creeping grains (almost-static layer, see Fig. 4).

5 Measurement analysis

5.1 Statistics

The raw data out of the photomultiplier were analysed to identify the burst signals, then, after filtering and validating the bursts, the mean velocity and the variance are obtained as moments of the velocity probability distribution. Three different kinds of average are possible with the software packages included in our LDV system: an unweighted average:

$$< U >_{\mathrm{un}} = \frac{\sum_{i=1}^{N} u_i}{N}$$

u_i velocity detected for each validated burst;

N number of burst in the sample;

a weighted average using transit time:

$$< U >_{\mathrm{wtt}} = \frac{\sum_{i=1}^{N} \Delta t_i u_i}{\sum_{i=1}^{N} \Delta t_i}$$

$\Delta t_i =$ persistence time of the ith burst;

a weighted average using arrival time:

$$< U >_{\mathrm{wat}} = \frac{\sum_{i=1}^{N} (t_i - t_{i-1}) u_i}{\sum_{i=1}^{N} (t_i - t_{i-1})}$$

where t_i is the starting time of the ith burst.

The first two averages are essentially coincidental, the third average shows negligible differences with the first two if the measurement volume is in a region permanently occupied by particles. In regions where particles are often absent, a notable deviation is observed.

The unweighted average is intrinsically more similar to the phasic average, and has been adopted in the present data elaboration.

5.2 Velocity distribution

The drum was operated at 2 and 5 rpm. The measurements of the velocity were performed in three vertical

sections, the central one through the axis of rotation (midsection), the other two at a distance of 65 mm upstream (upper section) and downstream (lower section), Fig. 2. In the midsection, the granular stream is non-accelerated, whereas in the upper and in the lower sections the stream accelerates and decelerates, respectively. The geometric characteristics of the stream are evaluated through visual observations and the analysis of the velocity profiles.

The motion of the plug flow is well defined, with the velocity vector tangent to coaxial circles and the modulus equal to ωr, where ω the angular speed and r is the distance from the rotation axis. Every distortion of this motion is due to a flowing layer or to some secondary phenomena, such as percolation of small particles. The effects of percolation are quantitatively modest: the small particles move through the meanders between the big particles and tend to segregate in the lowest part of the drum, with a measured vertical velocity of percolation of a few millimetres per second (we cannot find any reason for the existence of a horizontal percolation nor it was observed). The distortion point of the velocity profile from a linear distribution is denoted as the "measured bottom"

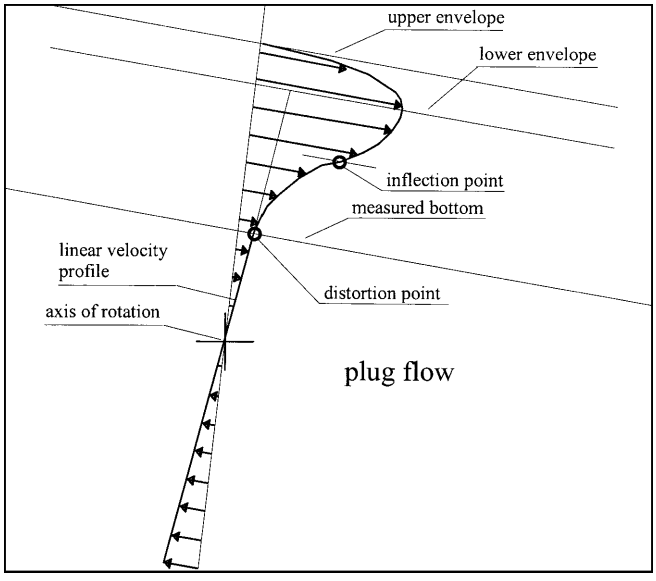

Fig. 5. Qualitative velocity profile in the plug flow and in the flowing layer and characteristic points

and is assumed as the indicator of the maximum extent of the flowing layer (Fig. 5).

The thickness of the flowing layer measured in this way is higher than that measured through visual observations. The differences are due to the fact that the computed layer refers to measurements performed $\sim 2d$ (where d is grain diameter) deep inside the drum, while the observed layer is essentially the layer in contact with the glass. Moreover, it is difficult to note small velocity gradients by eye. Roughly speaking, the observed bottom can be considered as limiting the flowing layer, whereas the area between the observed bottom and the measured bottom can be considered as the almost-static layer.

A list of the relevant geometrical characteristics for 1.2–1.7 mm sand grains flowing in the drum operated at 5 rpm is reported in Table 2. The measurement results for the other tested materials are reported in Longo and Lamberti (1998). The maximum computed thickness of the active layer is equal to about 17 grain diameters in the upper section, 23 grain diameters in the midsection and 15 grain diameters in lower section.

The distance between the upper and the lower free surface envelopes ranges from $4.5d$ to $4.9d$ and is a measurement of the amplitude of the longitudinal pulsation of the free surface. The pulsations are essentially generated by the impact of the grains on the roughened drum wall and travel with a higher amplitude downstream than upstream, ranging from 20% to 30% of the flowing layer thickness. The period of the main pulsation is of $\sim$3.6 s, as measured by a frame-by-frame observation of the video records.

If the direction along which velocity is measured is:

$$l_i = \{\cos\theta, \sin\theta\}$$

where θ is the angle in a reference system, the measured velocity is:

$$u_\theta = u_i l_i$$

where u_i are the two components of velocity in the reference system, and hence the mean observed velocity is:

$$\langle u_\theta \rangle = \langle u_i \rangle l_i$$

From two measurements at different angles θ, the two components $\langle u_i \rangle$ can be found.

In Fig. 6 the grain speed versus depth is reported for sand grains; only data between the free surface and the distortion point are shown. A more or less pronounced inversion of the velocity profile is evident between the two

Table 2. Observed geometric characteristics of the stream in the active layer: 1.2–1.7 mm sand grains, 5 rpm

	Unit	Upper section	Mid-section	Lower section
Observed bottom slope	°	49	33	32
Measured bottom slope	°	49	33	32
Free-surface upper envelope slope	°	45	35	40
Distance between the free-surface envelopes	mm	6.7 = 4.5d	7.1 = 4.7d	7.4 = 4.9d
Distance between the mean free-surface envelope and the inflection point	mm	11.2 = 7.8d	12.5 = 8.7d	10.9 = 7.6d
Observed flowing layer thickness	mm	16.0 = 10.7d	23.0 = 15.3d	18.0 = 12.0d
Computed flowing layer thickness	mm	25.5 = 17.0d	34.0 = 22.7d	23.0 = 15.3d
Maximum shear rate	s^{-1}	48	79.3	62.7
Maximum velocity	m/s	0.62	0.66	0.65

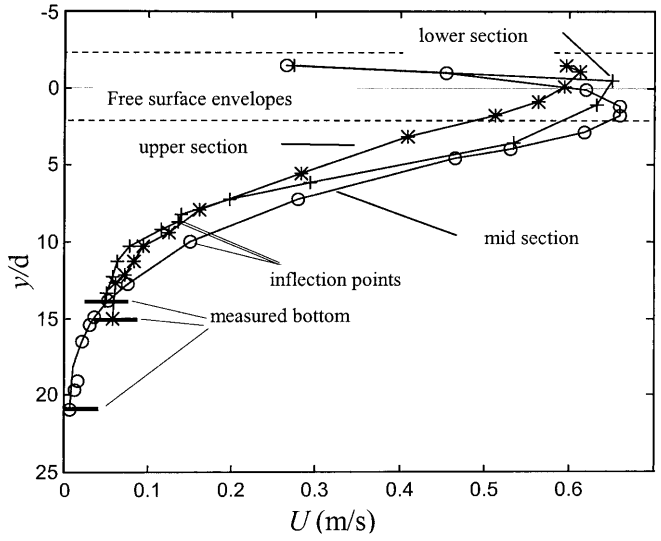

Fig. 6. Grain speed for the upper section (*), the midsection (o) and the lower section (+) for 1.2–1.7 mm sand grains, 5 rpm

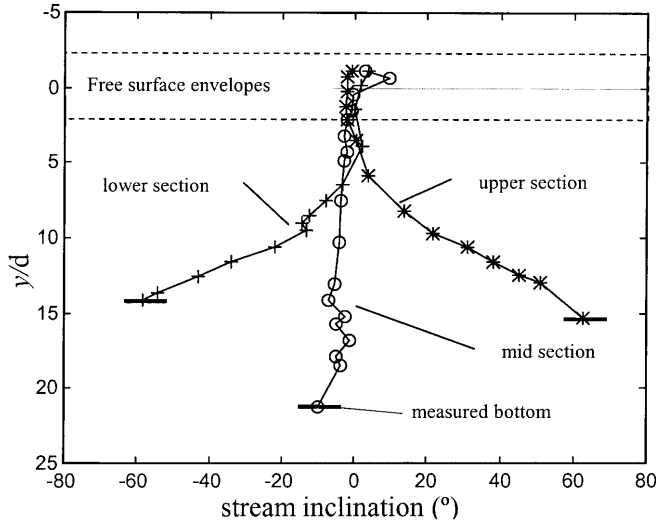

Fig. 7. Inclination of stream lines relative to current (*x*-axis in Fig. 4) for the upper section (*), the midsection (o) and the lower section (+) for 1.2–1.7 mm sand grains, 5 rpm

surface envelopes. This inversion could be a consequence of friction with air at the interface, even though it looks too notable, with a maximum of more than 50% in the midsection and a minimum of less than 10% in the upper section. In Fig. 7 the stream inclination is reported for the three sections.

If there are more than two measurements of the velocity, the two components that best fit the set of measurement equations can be evaluated, thereby also obtaining information on measurement errors.

In most experiments we simply measured the grain velocity in the horizontal and in the vertical direction at each location. Due to its length, the more detailed analysis has been applied only to 0.3–0.4 mm glass beads and 0.84–1.19 mm sand grains rotating at 2 rpm. For these two tests we carried out six measurements at each point along the vertical (1 mm step) with different angles (30° apart).

The results for one of the two tests are reported in Fig. 8. The velocity profiles obtained using this more detailed analysis show that the velocity profile is quite regular, with errors that are minor enough to be reasonably confident of the technique's reliability, Some small free-surface perturbations move upstream, with an amplitude of $\sim 3d$. The error bars are equal to plus/minus the computed square root of the variances of the partial regression coefficients.

5.3 Velocity covariance (temperature)

The model for velocity fluctuations is:

$$\left\langle u_\theta'^2 \right\rangle = \left\langle u_i' u_j' \right\rangle l_i l_j$$

From two orthogonal measurements the first invariant $\left\langle u_i' u_i' \right\rangle$ or "temperature" can be estimated:

$$T_x = \frac{\sum_{i=1}^{N} \left(u_{xi} - < U_x >_{\mathrm{un}}\right)^2}{N} \tag{2}$$

$$T_y = \frac{\sum_{i=1}^{N} \left(u_{yi} - < U_y >_{\mathrm{un}}\right)^2}{N} \tag{3}$$

$$T = T_x + T_y \tag{4}$$

From three measurements the whole covariance matrix can be estimated, and from more than three measurements it is also possible to estimate the measurement errors.

In Fig. 9 the granular temperature profiles (obtained through two orthogonal measurements) for the three sections in one of the experiments are shown. The granular temperature plays the same role as the thermodynamic temperature: the granular energy is generated by shear stress and is then diffused through collisions and kinetic flux. An over-generation in the intermediate region of the profile (where stress and strain are both intense) is expected, with a corresponding over-dissipation in the lower region, where the strain is reduced. The temperature increases down-slope and from the bottom to the free surface, with a small inversion near the free surface in the midsection and in the lower section.

As for the mean velocity, we performed a more detailed analysis of the velocity covariance tensor, extending the set of measurements for two experiments, with results for one of the two reported in Fig. 10. The error bars represent plus/minus the computed square root of the variances of the partial regression coefficients.

Measurements have also been carried out along a transverse profile on the free surface of the stream, in order to evaluate the distortion of the flow field due to the walls, see Fig. 11. The walls reduce the grain velocity and increase the pseudotemperature due to rebounding particles. The gradient of the velocity is very strong near the glass surface and makes the correct determination of the measurement volume position critical. Assuming that

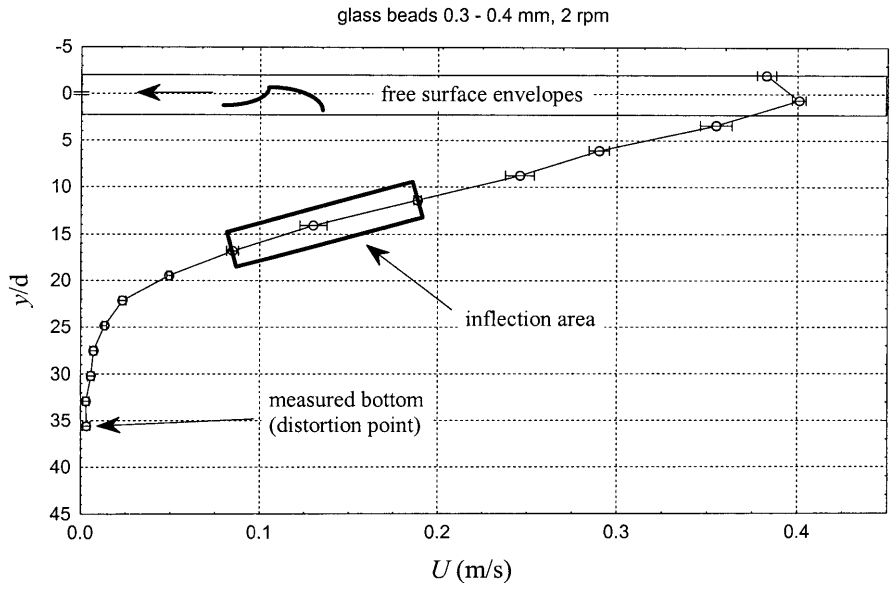

Fig. 8. Grain speed in the midsection; 0.3–0.4 mm glass beads, 2 rpm

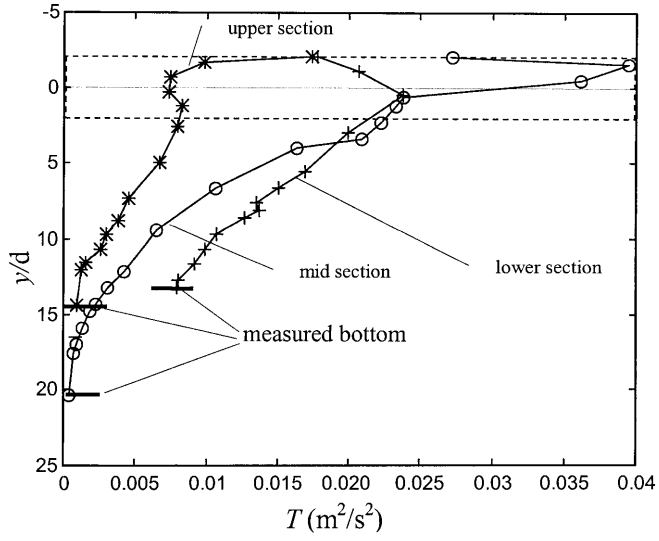

Fig. 9. Granular temperature for the upper section (*), the midsection (o) and the lower section (+) for 1.2–1.7 mm sand grains, 5 rpm

the penetration of the beams is of $\sim 2d$, an underestimation ranging from 10% to 20% of the mean velocity profile is expected in the upper and in the lower sections; a much smaller underestimation is expected in the midsection.

A more quantitative assessment of how much the low deviates from the bulk system is presented in Sect. 5.4 after discussing the volume discharge.

5.4
Grain volume concentration (data rate)

A third important state variable of the granular system is the local time-averaged concentration. In principle, it can be obtained from the (validated) data rate by formulating some hypothesis about the behaviour of particles moving through the measurement volume. If k is the number of bursts generated by a single particle, the mean distance between the centres of the particles is equal to $kU\Delta t$, where Δt is the average interval time between two sequential bursts, and U is the average velocity computed from the burst signals at that location. The mean distance between particle centres is related to the actual concentration v and to the maximum possible concentration v_o, the concentration at which the particles are in reciprocal contact, by the relation (Bagnold 1954):

$$l = d(v_o/v)^{1/3} \tag{5}$$

By equating this expression to the mean distance computed as $kU\Delta t$ we obtain:

$$v = v_o\left(\frac{kU\Delta t}{d}\right)^{-3} = v_o\left(\frac{nd}{kU}\right)^{3} \tag{6}$$

where n is the data rate.

Small errors in measuring the data rate and the variability of k strongly influence the estimation of the concentration. In isotropic conditions, without any directional structure of the particle system, the average distance between particles depends on concentration in a unique way. Some difficulties can arise because the number of bursts generated by a single particle is not constant, but depends on the particle size, shape, possibly on its rotation rate and on the roughness of its surface. The numerous uncertainties resulted in our performing some tests in order to evaluate empirically the value of k.

For particles of given size and shape, it is expected that k depends on particle velocity and particle concentration; in order to properly describe such dependence, a series of tests at different concentrations and different velocities had to be performed. Some preliminary tests with fixed known concentration were carried out by sticking grain particles on a sheet of paper. The concentration, computed by counting the number of particles per square centimetre and assuming that they are on a single layer having a thickness equal to the mean diameter, is equal to 0.45. The

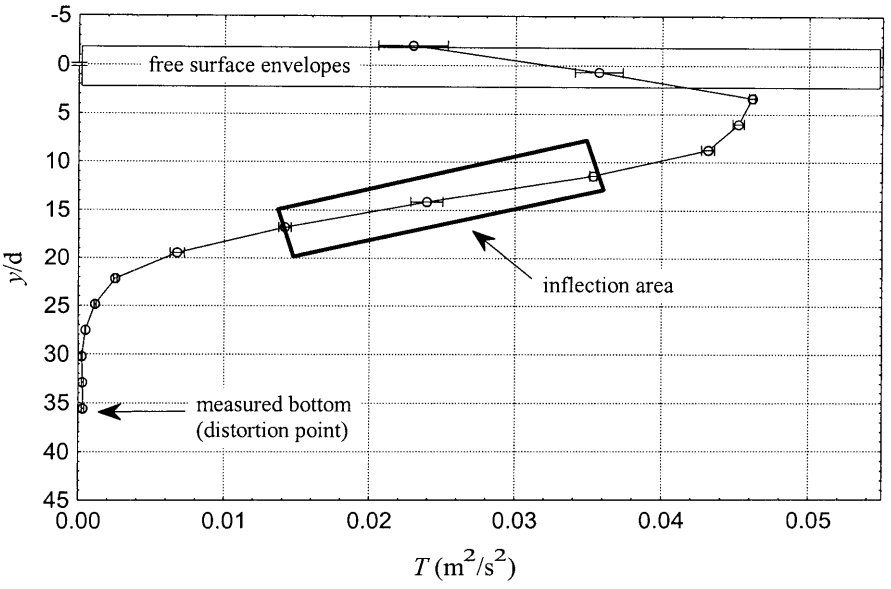

Fig. 10. Pseudotemperature in the mid-section for 0.3–0.4 mm glass beads, 2 rpm

sheet was moved at different speeds and the LD signal was collected and then elaborated using the three lower band filters, corresponding to measurable velocities in the range ±0.16 m/s, ±0.54 m/s and ±1.62 m/s.

The LDV system can show both the gross data rate (referred to all bursts in the scattered signal, independent on their validity) and the net data rate (referred only to validated bursts). The data rate is influenced by the voltage supply of the photomultiplier. In Fig. 12 the number of bursts k computed using the gross data rate versus the imposed mean velocity for the three different bands of measurements is shown at voltage equal to 800 V. The thick parts of the lines connecting the experimental points correspond to the range of relatively small variations of k.

Nevertheless, it is clear that using the gross data rate the variation of k is too high. Further analysis was performed examining the net data rate, i.e., the data rate of validated bursts. To account for dependence on photomultiplier voltage, the tests were repeated for three different voltages, i.e., 696 V, 800 V and 896 V and for the three different bands.

The results of the analysis performed only by taking into account the validated bursts are plotted in Fig. 13. The continuous lines connecting the points of measurement for the wider band (±1.62 m/s) show a substantial constant number of bursts scattered by each particle, independent of the grain speed and of the photomultiplier voltage supply, with a calibration function becoming a constant at ≈1 at a wide range of velocities. The dashed lines connect points of measurement for the two lower bands of velocity. Some outliers are present, and the results are very sensitive to the voltage supply of the photomultiplier.

These preliminary tests suggest that, in principle, it is possible to use the same data to compute both the grain velocity and the grain volume concentration, by selecting the proper calibration coefficient for the latter. It was judged better to collect the data for volume concentration separately using the wider band and a unique calibration function.

The grain volume concentration profiles for one of the tests are reported in Fig. 14. The heavy reduction of the volume concentration in the area occupied by the free surface oscillations is due to the frequent absence of mass flow.

The volume discharge in each section is based on the plug flow kinetics and can be expressed as:

$$Q_{v\mathrm{P}} = v_{\mathrm{o}} \frac{\omega}{2} \left(R^2 - r^2\right) \tag{7}$$

where r is the radial distance of the measured bottom in the section of interest. The volume discharge can also be computed as integral of the stream velocity:

$$Q_{v\mathrm{S}} = \int_{c.b.}^{u.e.} v U_x \mathrm{d}y \tag{8}$$

with the integral extended from the measured bottom to the upper envelope. An extreme hypothesis assumes a constant concentration, equal to the unconsolidated concentration at rest ($v_{\mathrm{o}} = 0.578$) from the measured bottom to the lower envelope, and a decreasing concentration from the lower envelope to the upper envelope:

$$Q_{v\mathrm{I}} = v_{\mathrm{o}} \left(\int_{c.b.}^{l.e.} U_x \mathrm{d}y + \int_{l.e.}^{u.e.} \gamma U_x \mathrm{d}y \right) \tag{9}$$

γ is an intermittence factor, whose the distribution is assumed to be linear between the two envelopes. The volume discharges computed using the three different approximations are reported in Table 3.

There is a discrepancy in the different values of the discharge. Amongst them, the most reliable is $Q_{v\mathrm{P}}$ because velocity in the plug is known using simple geometry and the possible sources of error are restricted to r and to v_{o}, whereas in $Q_{v\mathrm{S}}$ and in $Q_{v\mathrm{I}}$ the sources of error are the measured velocity, the grain volume concentration and the stream thickness. The main error source is the inaccuracy of the volume concentration measurements: the technique

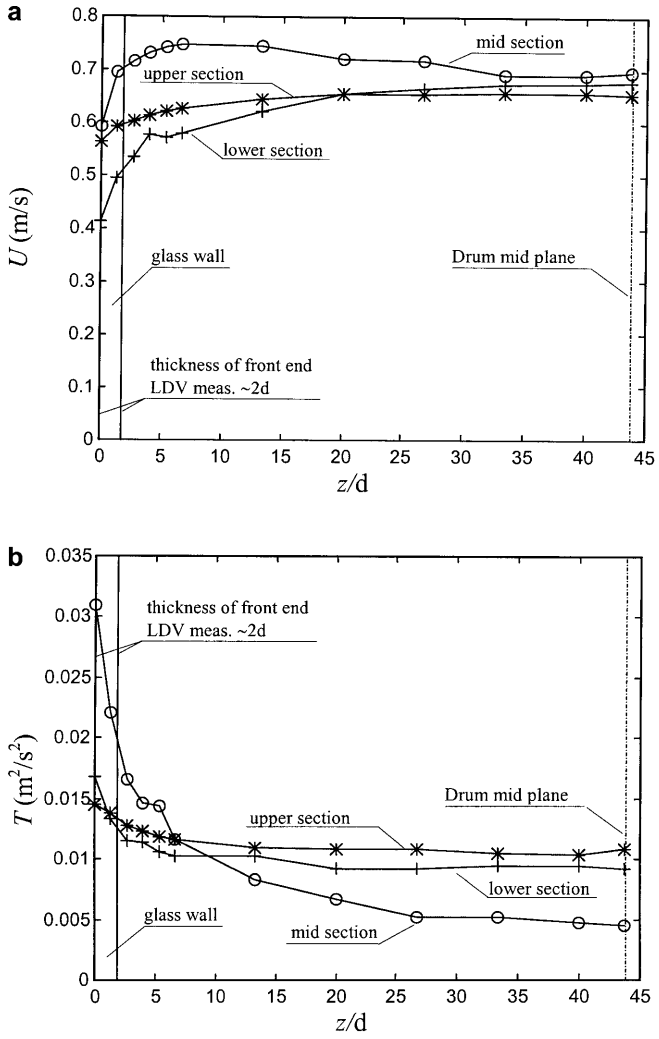

Fig. 11a,b. **a** Grain speed and **b** granular temperature in transverse direction at the upper section (*), the midsection (o), and the lower section (+) for 1.2–1.7 mm sand grains, 5 rpm

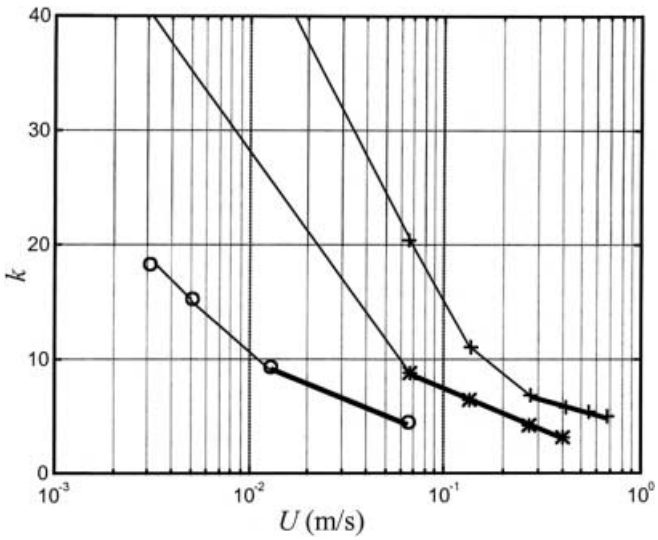

Fig. 12. Bursts per particle versus velocity for three different filter bands at a fixed concentration $\nu = 0.45$. Filter bands: (o) ±0.16 m/s, (*) ±0.54 m/s, (+) ±1.62 m/s

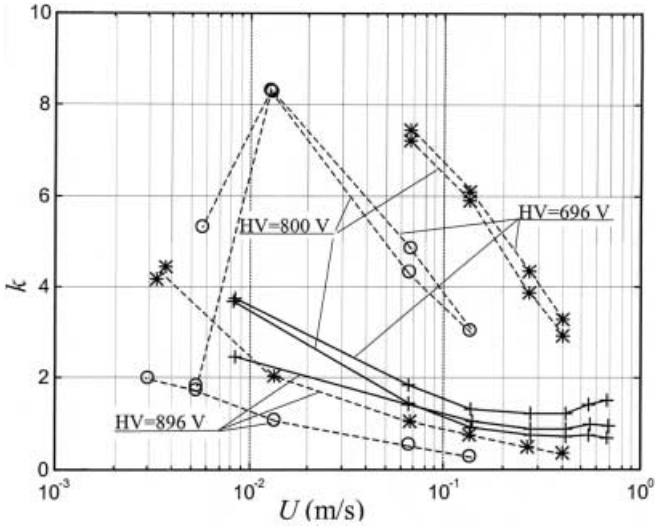

Fig. 13. Validated bursts per particle versus velocity for three different bands at a fixed concentration ν=0.45 and for different voltage supplies of the photomultiplier: (o) ±0.16 m/s, (*) ±0.54 m/s, (+) ±1.62 m/s

for measuring the grain volume concentration, although very promising, needs further improvement. The volume discharge $Q_{\nu I}$ underestimates the value of $Q_{\nu P}$ by ~20%. This could be a consequence of the measured grain velocity being less than the actual grain velocity in the midplane of the drum, especially at higher values, due to wall effects. We can infer that higher velocity in the midplane also means a thicker active layer.

6
The velocity covariance tensor

As discussed in Sect. 5.3, we were able to evaluate the velocity covariance tensor (which approximates the kinetic stress tensor) for two experiments. The computed principal axes of the velocity covariance tensor do not coincide with the principal axes of the rate of deformation tensor, as is evident in Fig. 15. We made an attempt to explain this result by considering the possible factors influencing the velocity covariance (or the pseudotemperature).

The orientation of the velocity covariance principal axes is affected by the pseudotemperature anisotropy. The principal axes are collinear with the principal axes of the rate of deformation tensor if pseudotemperature is isotropic and the cross-correlation terms are nonzero. The pseudotemperature is generated by the kinetic (or streaming) effect (the flux of particles carrying their own momentum in a region with different mean momentum) and by collisions. Streaming is responsible for anisotropy, with higher values of random velocity of particles in the direction of the mean motion (Campbell 1990). Some numerical results are available by Campbell (1989), who used computer simulation to evaluate the complete stress tensor, separating the kinetic (streaming) and the collisional components for rough inelastic spheres in an imposed simple shear flow. Using Campbell's results, we

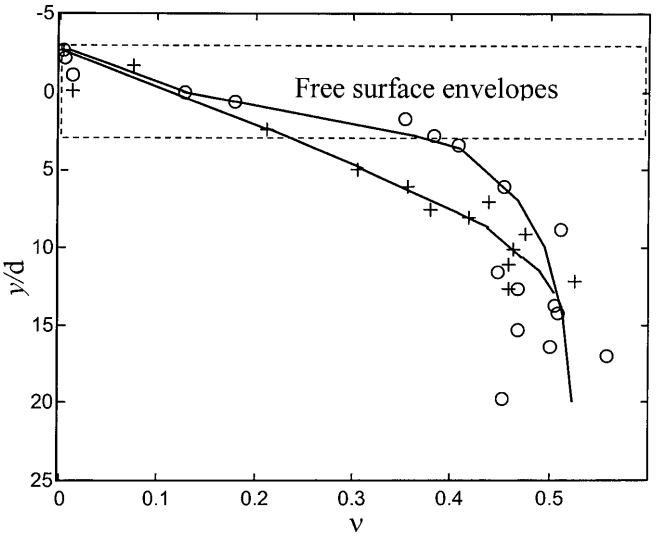

Fig. 14. Grain volume concentration in the midsection (o) and in the lower section (+) for 1.2–1.7 mm sand grains, 5 rpm

Table 3. Computed volume discharge: 1.2–1.7 mm sand grains, 5 rpm

	Q_{vP} (v_9 = 0.578) m^2/s	Q_{vS} m^2/s	Q_{vI} (Linear intermittence factor, v_o = 0.578) m^2/s
Upper section	4.55×10^{-3}	–	4.10×10^{-3}
Midsection	5.75×10^{-3}	3.80×10^{-3}	4.70×10^{-3}
Lower section	4.88×10^{-3}	3.22×10^{-3}	4.00×10^{-3}

computed the orientation of the principal axes, as shown in Fig. 16, for varying volume concentrations and elastic restitution coefficient e. The quantity $\Delta\theta$ is the angle between the nearest principal axes of the velocity covariance and the rate of deformation tensor.

The effects of pseudotemperature anisotropy are more evident at low concentration and low elastic restitution coefficient. A rapid increase of the relative angle $\Delta\theta$ is experienced beyond a critical value of volume concentration v, with an asymptotic value $\Delta\theta = 90°$ (i.e., colinearity of the principal axes) at high values of the volume concentration, where collisions dominate and streaming has a negligible effect. Considering only the anisotropy due to streaming can give only a partial justification of the large angle (≈41°) detected in our experiments.

Among the other possible factors influencing the velocity covariance, we considered the effect of the free-surface small perturbations moving slowly upstream, which are able to enhance the variance of velocity in the stream direction. In the following analysis, the distortion of the pseudotemperature field due to this perturbation is evaluated.

The mass conservation equation for the grains, assuming a constant and uniform grain volume concentration and neglecting the velocity component along y, reads:

$$\frac{\partial \eta}{\partial t} + \frac{\partial (h+\eta) u_x}{\partial x} = 0 \tag{10}$$

where η is the instantaneous free surface level, h is the stream height and u_x is the instantaneous velocity component along x. Expressing u_x as a time-averaged value plus a fluctuation $\overline{U}_x + u'_x$, and neglecting the lower-order terms, the mass balance equation reads:

$$\frac{\partial \eta}{\partial t} + \overline{U}_x \frac{\partial \eta}{\partial x} + h \frac{\partial u'_x}{\partial x} = 0 \tag{11}$$

Assuming perturbations of constant shape moving with absolute celerity $\overline{U}_x \pm c$ results:

$$\frac{\partial \eta}{\partial t} = -\left(\overline{U}_x \pm c\right) \frac{\partial \eta}{\partial x} \tag{12}$$

and substituting (12) into (11):

$$\frac{\partial \eta}{\partial x} = \pm \frac{h}{c} \frac{\partial u'_x}{\partial x} \tag{13}$$

Integrating and calculating the root-mean-square of the free-surface level and of the fluctuating velocity, results in:

$$\eta_{\mathrm{rms}} = \frac{h}{c} \left(u'_x\right)_{\mathrm{rms}} \tag{14}$$

It can be assumed that η_{rms} is equal to one-quarter the distance between the free surface envelopes, i.e., $0.75d$ for glass beads at 2 rpm. The observed celerity of the perturbations is roughly equal to the mean flow velocity (the perturbations are slowly moving upstream): $c \cong 0.3$ m/s, and the stream height is of the order of $15d$. Substituting this into (16) we obtain $\left(u'_x\right)_{\mathrm{rms}} = 0.015$ m/s.
This value favourably compares with the measured velocity reduction near the free surface, but is not high enough to justify the measured rotation of the axes. In fact, the strongly oriented and anisotropic pseudotemperature field induced by small perturbations can be expressed as a tensor:

$$\boldsymbol{W} = \begin{bmatrix} \left(u'_x\right)^2_{\mathrm{rms}} & 0 \\ 0 & 0 \end{bmatrix} \tag{15}$$

while the pseudotemperature tensor, thought of as an isotropic function of the velocity of deformation tensor, has the principal axes at 45° in respect to the stream orientation and reads:

$$\boldsymbol{K} = \frac{1}{2} \begin{bmatrix} M+m & m-M \\ m-M & M+m \end{bmatrix} \tag{16}$$

where M and m are the maximum and the minimum components. Adding the two tensors we obtain:

$$\boldsymbol{K} + \boldsymbol{W} = \frac{1}{2} \begin{bmatrix} M+m+2\left(u'_x\right)^2_{\mathrm{rms}} & m-M \\ m-M & M+m \end{bmatrix} \tag{17}$$

with orientation of the principal axes expressed as:

$$\varphi = \frac{1}{2} \tan^{-1} \left(\frac{m-M}{\left(u'_x\right)^2_{\mathrm{rms}}} \right)$$

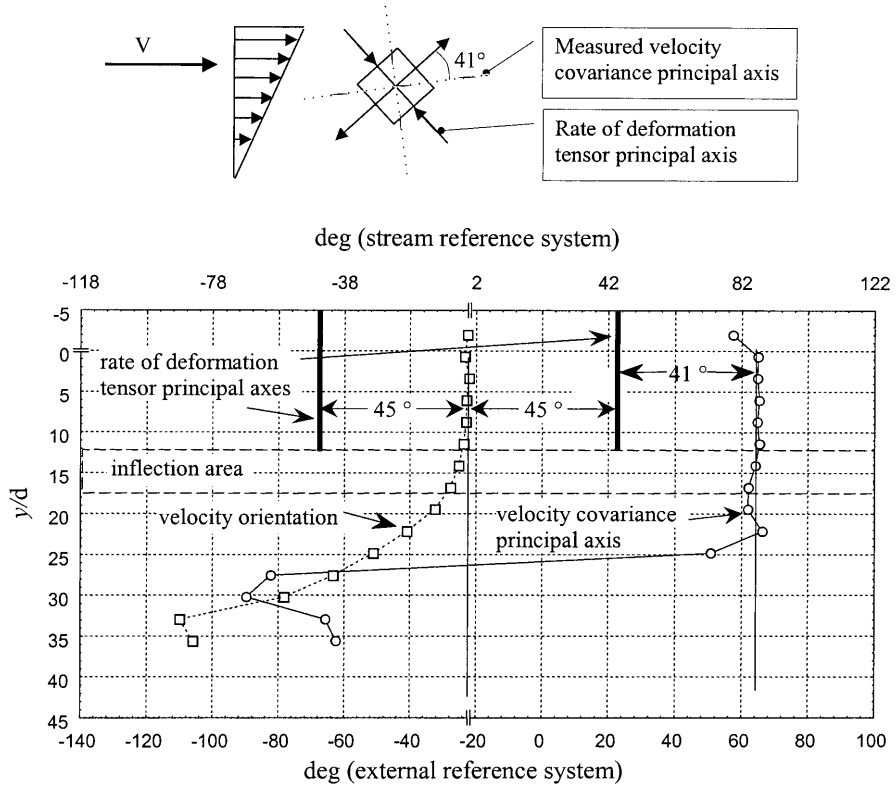

Fig. 15. Principal axes of the velocity covariance and the rate of deformation tensor for 0.3–0.4 mm glass beads, 2 rpm, midsection

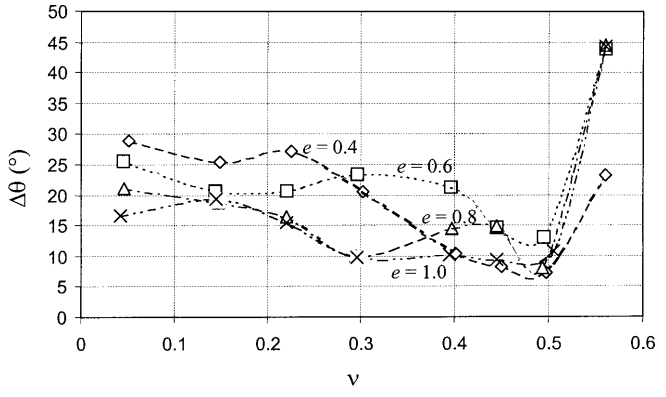

Fig. 16. Angle between the nearest principal axes of the velocity covariance and the rate of deformation tensor for rough inelastic spheres with variable elastic restitution coefficient e in a simple shear flow. Data elaborated from Campbell (1989)

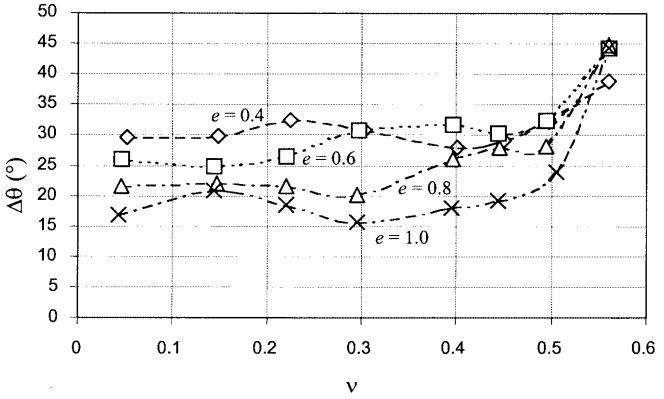

Fig. 17. Angle between the nearest principal axes of the velocity covariance and the rate of deformation tensor introducing an extra stress in the flow direction due to free-surface perturbation for rough inelastic spheres with variable elastic restitution coefficient e in a simple shear flow. Data elaborated from Campbell (1989)

in the chosen coordinate system. As expected, φ is equal to 45° in the absence of induced pseudotemperature fluctuations and tends to zero because of small differences between the maximum and the minimum component of $\boldsymbol{K}$ or the high value of the perturbation-induced pseudotemperature.

Applying such a scheme to 0.3–0.4 mm glass beads rotating at 2 rpm, we obtain a rotation of the axes due to the pseudotemperature fluctuations equal to ≈12° near the free surface, but only of ≈6° for most height levels, far from the measured value of ≈41° (see Fig. 15).

Including both effects, the anisotropy due to streaming and to free surface perturbation, the experimental results can be better interpreted. Adding to Campbell's results the effect of an additional contribution in the mean flow direction due to a fluctuating velocity $\left(u_x'\right)_{\mathrm{rms}} = 0.015$ m/s, we obtain the results reported in Fig. 17.

The angle separation between principal axes $\Delta\theta$ is still below the measured angle of 41°, but we achieved an interpretation of a uniform value more or less independent of the grain volume concentration.

The same measurements and analysis were carried out for sand grains; the results, reported in Longo and Lamberti (1998), show a measured rotation of the covariance velocity equal to ≈23°. This value, while smaller than for glass beads, is still not justified simply by the

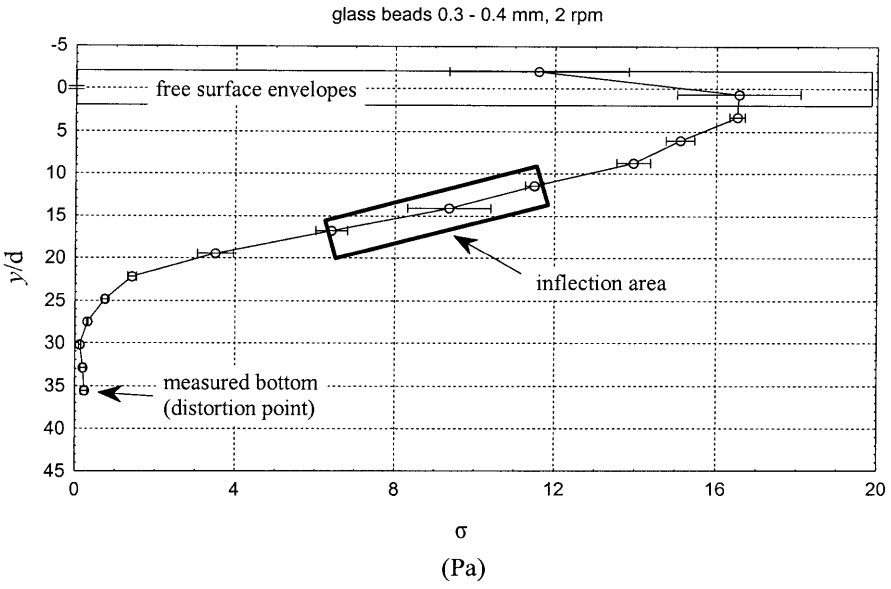

Fig. 18. Normal kinetic stress ($\propto T_y$) in the midsection for 0.3–0.4 mm glass beads, 2 rpm

estimated anisotropy in the pseudotemperature field induced by surface perturbations and is quite well interpreted by both streaming and free-surface perturbation-induced anisotropy.

We can conclude that in the stream core, the velocity covariance is a nonisotropic function of the velocity deformation tensor due to streaming and free surface perturbations effects, or that it depends on gravity or also on the global stress tensor. However, it must also be stressed that there is not enough knowledge of perturbation dynamics to draw firm conclusions.

7 Stress

Assuming a uniform grain volume concentration, it is possible to compute the normal kinetic stress σ_{kyy} and the orientation of the principal axes (see Fig. 18). The error is only relevant in the upper layer near the free surface.

The measured pseudotemperature and shear rate have also been used to evaluate the corresponding kinetic and collisional tangential stress according to the model of Lun et al. (1984). According to this model, the kinetic plus collisional tangential stress is:

$$\tau_{kc} = \rho_s f_2(v, e, d)\sqrt{T}\frac{\partial U}{\partial y} \tag{19}$$

where e is the elastic restitution coefficient and d is the grain diameter.

The experiments results have been interpolated and smoothed through a polynomial fitting. In Fig. 19 this stress is plotted in comparison with the global tangential stress, calculated assuming a uniform grain volume concentration. The difference between the global tangential stress and the kinetic + collisional tangential stress is the frictional contribution, which seems to be the main stress in most of the flowing layer.

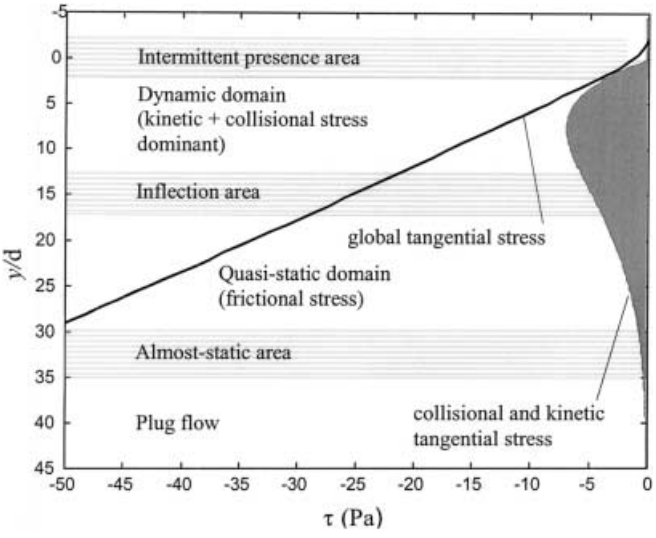

Fig. 19. Tangential collisional and kinetic stress computed using the experimental output in the model of Lun et al. (1984), midsection, 0.3–0.4 mm glass beads, 2 rpm

8 Conclusions

Experiments and an analysis of results show that measurements of granular flows velocity using LDV give substantially correct results, with an underestimation of velocity due to the effect of the wall surface.

The grain volume concentration measurements using the LD signal are promising, although calibration and further improvements are necessary to obtain correct results. The volume discharge calculated using the experimental values is lower than the expected discharge.

By observing the measured velocity profiles, three regions can be detected in a rotating drum partially filled with grains: a plug flow, with a circular path of the locked particles, an almost-static layer and a flowing layer. In the flowing layer the inflection area separates an upper collision-dominated flow domain from a lower friction-dominated domain. Velocity profiles are not suitable to define the inflection area, whereas temperature profiles have

proved to be better indicators: in the inflection area, the temperature shows an abrupt drop.

The free surface is perturbed by oscillations slowly moving upstream or downstream, depending on the experiment conditions, with an amplitude of a few grain diameters. As a consequence, the mean velocity is increased or decreased in the envelope area.

The granular temperature, related to the velocity variance, increases from the bottom to the free surface. The velocity covariance tensor is not collinear with the deformation velocity tensor, with a higher rotation for spheres than for sand grains. The phenomenon can be partly explained by considering the anistropy due to streaming and free-surface perturbations.

A comparison between the global stress and the kinetic + collisional stress calculated using the model of Lun et al. (1984) reveals that most of the stress is frictional in and below the inflection area.

References

Ahn H, Brennen CE, Sabersky RH (1991) Measurements of velocity, velocity fluctuation, density and stresses in chute flows of granular materials. J Appl Mech 58: 792–803

Anderson GK, Jackson R (1992) A comparison of the solutions of some proposed equations of motion of granular materials for fully developed flow down inclined planes. J Fluid Mech 241: 145–168

Bagnold RA (1954) Experiments on a gravity-free dispersion of large solid spheres in a Newtonian fluid under shear. Proc R Soc Lond A 225: 49–63

Boateng AA, Barr PV (1997) Granular flow behaviour in the transverse plane of a partially filled rotating cylinder. J Fluid Mech 330: 233–251

Campbell CS (1988) Boundary interactions for two-dimensional granular flows: asymmetric stresses and couple stresses. In: Satake M, Jenkins JT (eds) Micromechanics of granular materials. Elsevier, Amsterdam, pp.163–174

Campbell CS (1989) The stress tensor for simple shear flows of a granular material. J Fluid Mech 203: 449–473

Campbell CS (1990) Rapid granular flows. Ann Rev Fluid Mech 22: 57–92

Campbell CS, Gong A (1986) The stress tensor in a two-dimensional granular shear flow. J Fluid Mech 164: 107–25

Gutt G, Haff PK (1991) Boundary conditions on continuum theories of granular flow. Int J Multiphase Flow, 17: 621–634

Hui K, Haff PK, Ungar JE, Jackson R (1984) Boundary conditions for high-shear grain flows. J Fluid Mech 145: 223–233

Jenkins JT, Askari E (1991) Boundary conditions for granular flows: phase interfaces, J Fluid Mech 223: 497–508

Jenkins JT, Richman MW (1985) Kinetic theory for plane flows of a dense gas of identical, rough, inelastic, circular disks. Phys Fluids 28: 3485–3494

Jenkins JT, Richman MW (1986) Boundary conditions for plane flows of smooth, nearly elastic, circular disks. J Fluid Mech 171: 53–69

Jenkins JT, Savage SB (1983) A theory for the rapid flow of identical, smooth, nearly elastic particles. J Fluid Mech 130: 187–202

Johnson PC, Jackson R (1987) Frictional–collisional constitutive relations for granular materials with application to plane shearing. J Fluid Mech 176: 67–93

Johnson PC, Nott P, Jackson R (1990) Frictional–collisional equations of motion for particulate flows and their applications to chutes. J Fluid Mech 210: 501–535

Longo S, Lamberti A (1998) Grain shear flow in a rotating drum. In: Debris flow management and risk assessment in the Alpine region, Final report, Vol. 2, University of Bologna, Italy, pp 2.9.1–2.9.39

Lun CKK, Savage SB, Jeffrey DJ, Chepurniy N (1984) Kinetic theories for granular flow: inelastic particles in Couette flow and slightly inelastic particles in a general flow field. J Fluid Mech 140: 223–256

Nott P, Jackson R (1992) Frictional–collisional equations of motion for granular materials and their applications to aerated chutes. J Fluid Mech 241: 125–144

Pasquarell GC, Ackermann NL (1989) Boundary conditions for planar granular flows. J Eng Mech 115: 1283–1302

Savage SB (1979) Gravity flow of cohesionless granular materials in chutes and channels. J Fluid Mech 92: 53–96

Seminara G, Tubino M (1993) Debris flows: Meccanica, controllo e previsione. Gruppo Nazionale per la difesa delle catastrofi idrogeologiche, CNR (in Italian)

Walton OR, Braun RL (1986) Stress calculations for assemblies or inelastic spheres in uniform shear. Acta Mech 63: 73–86